Wake Development of Airfoils with Serrated Trailing Edges

Xiao Liu*, Hasan Kamliya Jawahar† and Mahdi Azarpeyvand‡
University of Bristol, Bristol, United Kingdom, BS8 1TR

Wake development and aero-acoustic performance of airfoils fitted with trailing-edge serrations have been studied experimentally. A symmetric (NACA 0012) and an asymmetric (NACA 65(12)-10) airfoil with different types of trailing-edge serrations have been tested over a wide range of angles of attack and Reynolds number. The steady aerodynamic force measurements have shown that the use of trailing edge serrations leads to significant reduction of lift coefficient at low angles of attack. Particle Image Velocimetry (PIV), two-dimensional Laser Doppler Anemometry (LDA) and hot-wire measurements were carried out in order to improve our understanding of the wake development and the energy content of the turbulent coherent structures. Significant reduction in the airfoils wake turbulence level has been observed, cause may include the interaction between the flow field over the tip and root planes and three dimensional horse-shoe and streamwise structures in the near wake. Results have also shown that the use of slotted sawtooth reduction can lead to significant reduction of turbulent kinetic energy and Reynold's shear stress in the near wake region. The reduction of turbulence within the wake can significantly reduce the turbulence interaction noise in contra-rotating propellers, rotor-stator configurations, etc.

Nomenclature

$2h$	=	amplitude of serration
AoA	=	angle of attack
c	=	chord length
C_D	=	drag coefficient
C_L	=	lift coefficient
$C_{L,max}$	=	maximum lift coefficient
d	=	slot width
H	=	slot depth
Re_c	=	chord based Reynolds number
TE	=	trailing edge
TKE	=	turbulence kinetic energy
U	=	flow speed
U_0	=	free stream wind speed
$\overline{u'u'}$	=	streamwise Reynolds normal stress
$\overline{v'v'}$	=	spanwise Reynolds normal stress
$\overline{u'v'}$	=	Reynolds shear stress
α	=	angle of attack
α_s	=	serration angle
λ	=	serration wavelength

*PhD Student, Department of Mechanical Engineering, AIAA Student Member, xiao.liu@bristol.ac.uk
†PhD Student, Department of Aerospace Engineering, AIAA Student Member, hasan.kj@bristol.ac.uk
‡Senior Lecturer and Royal Academy of Engineering research fellow, Department of Mechanical Engineering, m.azarpeyvand@bristol.ac.uk

I. Introduction

THE increasing popularity of air travel and rapid growth in the number of airports close to the city limits have increased noise pollution leading to negative physiological and psychological effects on the surrounding residents. Therefore, stringent standards have been set by ICAO for aircraft noise control, attracting researchers interest to aero-acoustics. Noise generated from aircraft can be broadly classified in the airframe noise and engine noise. The engine noise has been reduced considerably over the last half century by the introduction of high bypass ratio turbofan engines and introduction of chevrons in the back of the nacelle and the engine exhaust nozzle. However, the reduction of broadband noise component from the compressor, due to the interaction of laminar and turbulent flows with blades, has remained a challenging task. It is also believed to play a significant role in the overall engine noise [1] and also in noise created from contra rotating propellers.

One of the dominant causes of airfoil self noise is the interaction of the airfoil surface with the turbulence produced by its own boundary layer, thus the turbulence intensity of the inflow and the interaction of turbulence at the boundary layer with the airfoil trailing-edge plays a major role in airfoil self noise [2]. The trailing edge noise is significant at low Mach numbers due to the efficient scattering of the turbulent fluctuations over a solid trailing edge [3]. In order to reduce this dominant trailing edge noise several passive methods such as serrated trailing edge [4–23], porous surface [15,24] and brushes [25,26] have been investigated over the past two decades. In particular, serrated trailing edges have been of significant interest amongst the research carried out on passive trailing edge treatments. Initially analytical investigations by Howe [4] have showed that simple modifications such as sawtooth and sinusoidal serrations to the trailing edge could reduce the intensity of the trailing edge radiation and the magnitude of reduction depends upon the frequency and the length and spanwise spacing of the teeth. Further experimental investigation [11, 12, 14, 15, 27] showed that the serrated trailing edge inserts can achieve a self-noise reduction of up to 2 and 6 dB with significant reduction at high frequencies whilst maintaining an acceptable aerodynamic performance. The more recent experiments showed that further noise reduction can be achieved by the use of more complex trailing edges such as: slitted edge, sawtooth with hole, slitted-sawtooth edge and randomly serrated trailing edges, etc. Even though trailing edge serrations have proven to be valid means of airfoil noise reduction, the mechanism in which it occurs is not completely understood. Therefore, detailed study of the aerodynamic performance, wake development, turbulence level and noise reduction source of treated airfoils have been carried out in order to better understand the noise reduction mechanism.

The presented paper is a detailed study of the wake development and aero-acoustic behaviour of airfoil with and without trailing edge serrations. Aerodynamic force measurements were carried out for a wide range of angles of attack and Reynolds number have been performed. The flow measurements have been carried out using methods such as PIV, LDA and hot-wire. The wind tunnel and experimental setup along with the measurement techniques employed in the current study are discussed in Sec .II. The results for force measurements, wake development and the wake energy content has been discussed in Sec .III.

II. Experimental and Computational Setup

A. Wind Tunnel and Experimental Setup

A comprehensive study of the aerodynamic performance for a symmetrical NACA 0012 and a cambered asymmetrical NACA 65(12)-10 airfoil with and without trailing edge serrations were performed in three different wind tunnels at University of Bristol. The wind tunnels were: (i) large low speed closed-circuit wind tunnel with an octagonal working section of 2.1 m $\times$ 1.5 m $\times$ 2 m, contraction ratio of 3:1 and a stable velocity range of 10 m/s to 60 m/s; (ii) low turbulence closed-circuit wind tunnel with an octagonal working section of 0.8 m $\times$ 0.6 m $\times$ 1 m, contraction ratio of 12:1, maximum velocity of 100 m/s and with turbulence level as low as 0.05%; (iii) open jet wind tunnel with diameter of 1.1 m, maximum reliable speed of 30 m/s and minimum turbulence level of 0.05%.

1. Force Measurements Setup

The aerodynamic lift and drag forces for both the airfoils were tested in the closed-circuit large low speed wind tunnel. To reduce the probable three-dimensionality effect associated with vortex shedding and drag, clear circular Perspex end-plates with a diameter 0.34 m were used on the airfoil to induce two-dimensionality. The edges of these circular end-plates were chamfered to reduce flow distortion. The spacing between the sides of the end-plates to the airfoil has a ratio of more than seven, as suggested by Boutilier [28], in order to obtain accurate measurements of lift forces and vortex shedding frequencies. The force measurements were taken using AMTI OR6-7-2000 force balance. This force balance measures the aerodynamic forces by passing a voltage induced by the force balance through AMTI MSA-6 strain gauge amplifier, which is then converted into force (N) using the builtin control system provided in the LabVIEW system design software. A thorough data independency test using different sampling frequencies was

carried out before choosing a sampling frequency of 37 Hz which provided the best data independency and least uncertainty in the results [29]. The final data sets were collected for a time period of 30 s and the post-processed results are presented in Section III.

2. *Particle Image Velocimetry Setup*

The wake development and the energy content of the turbulence structure within the wake of the airfoils were studied using two-dimensional two-component Particle Image Velocimetry. The laser sheet with a thickness of 1 mm was created using a Dantec DualPower 200 mJ Nd:YAG laser with a wavelength of 532 nm, the time interval between each snapshots were 15 μs with a repetition rate of 25 Hz. A mixture of Polyethylene glycol 80 with a mean diameter of 1 μm were used to seed the air inside the low turbulence windtunnel. A total number of 1600 images were captured using a FlowSense 4 MP CCD camera with a resolution of 2078×2078 pixels and 14 bit corresponding to field view of 11.3 cm×11.3 cm. The images were analysed with the DynamicStudio software from Dantec. The iterative process yeild grid correlation window of 16×16 pixels with an overlap of 50% resulting in a facial vector spacing of 0.43 mm.

3. *Hot-Wire Anemometry Setup*

Flow steady and unsteady velocity field measurements were carried out using single and cross-wire constant temperature hot-wire anemometry. Flow measurements were taken using Dantec 55P16 single sensor hot-wire probes with a 5 μm diameter and 1.25 mm long platinum-plated tungsten wire sensor for streamwise component. Dantec 55P51 gold-plated cross-wire probe with two 3 mm long platinum-plated tungsten wire sensors with 5 μm diameter placed 90° to each other were used for simultaneous measurement of normal and streamwise velocity components. The hot-wire probes were driven by Dantec StreamlinePro CTA 91C10 modules and controlled through a National Instrument NI9215 four channel module. Both hot-wire probes were calibrated using the Dantec 54H10 two point mode hot-wire calibrator. A yaw calibration for the cross-wire was performed between the angle of 45° and −45° in order to determine the relationship between the effective cooling velocity for each wire and the velocity components u and v. The flow field measurements were logged at a frequency of 20 kHz. The hot-wire probes were placed on 1 m long steel rod that was connected to the traverse system that was placed away from the flow field and traverse system was controlled using Matlab. The traverse system was placed away from the wind tunnel as to not influence the flow field and blockage of the tunnel flow.

4. *Laser Doppler Anemometry Setup*

Two component LDA measurements with 6-Watt argon-ion laser were performed within the wake of the airfoils. The system was operated in backscatter mode with a focal length of 600 mm. Velocity components were measured at the orthogonal intersection of the dual-green 514.5 nm and dual-blue 488.0 nm laser beams. The measurement volume at the beam intersection was a prolonged spheroid shape with diameter of 0.16 mm and length 2.9 mm. The system is mounted on a fully automated traverse system and controlled by inbuilt software package by Dantec (Burst Wave) used for data collection and post processing.

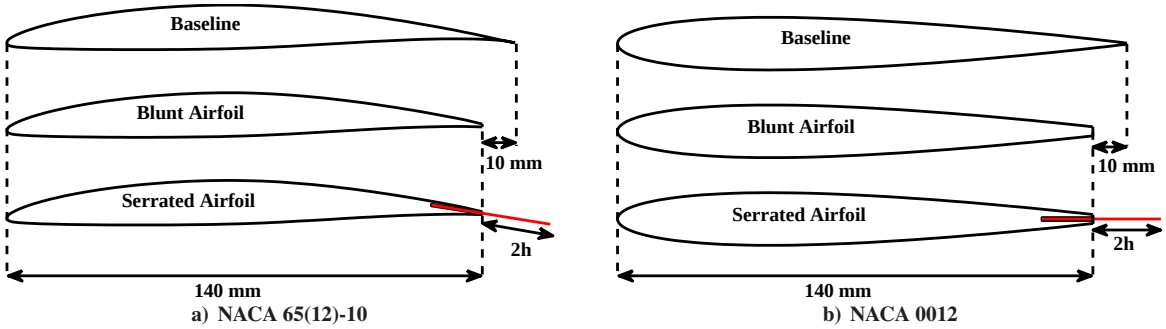

Fig. 1. Airfoil configurations employed in the current study

B. Serration Setup

The airfoils were manufactured using RAKU-TOOL® WB-1222 polyurethane board and machined using a computer numerical control (CNC) machine. Both the airfoils were designed with a 1.5 mm blunt trailing-edge with a slot that had a depth of 15 mm and thickness of 0.8 mm along the span-wise direction, as shown in Fig. 1 for the purpose of installing flat plate serrations at the trailing-edge. There is no general consensus in the literature as to how to define the trailing-edge serrations. There are two methods previously used by researchers: (i) to use the serration as a simple flap to the existing airfoil which increases the airfoil surface area and (ii) to keep the airfoil surface area constant as suggested by Gruber [5, 11–13]. In order to understand the effects of both treatments two different baselines have been considered in this study. The Blunt airfoil uses the serrations as an additional flap configuration (thus increasing the airfoil surface area), whereas the Baseline airfoil is designed to have the same surface area as that of the serrated airfoil as shown in Fig. 1.

The airfoil geometries shown in Fig. 1a and 1b have a span length of $L = 0.45$ m but with varying chord lengths. The Blunt airfoil has a chord length of $c = 0.14$ m with no trailing edge flat plate inserts. Baseline airfoil has a slightly different chord length that was achieved by a flat plate inserts without serrations at the trailing-edge of the Blunt airfoil. This increases the effective chord length to $c = 0.155$ m and thus increases the surface area of the airfoil.

Two types of serrations based on their good noise reduction performance from previous analytical and experimental studies [1, 4, 5, 11–13] were selected for the present study. The two types of serrations tested and presented here are the *sawtooth serration* (Fig. 2a) and *slotted-sawtooth serration* (Fig. 2b). In order to cover a wide range of serration angles geometrical parameters of the serrations such as the amplitude $2h$, periodicity wavelength λ, angle of serration edge α_s, slot width d and slot depth H were varied. The selected parameters presented in Table. 1 are due to their excellent noise reduction performance as demonstrated in previous experiments [5, 11–13]. Even though a variety of serration geometrical parameters were used for experimentation, only a few serrations are presented in this paper shown in Table. 1.

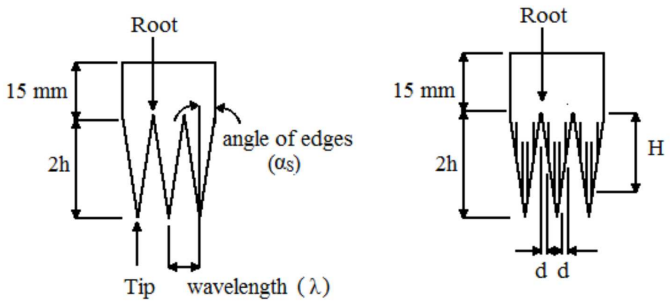

a) Sawtooth **b) Slotted-sawtooth**

Fig. 2. Serrated trailing-edge treatments tested in the current study

Table 1. Geometrical parameters of trailing-edge serrations.

Configuration	Serration Types	$2h$ (mm)	λ (mm)	λ/h -	α_s (deg.)	d (mm)	H (mm)
Case 1	Baseline 1	0	-	-	-	-	-
Case 2	Baseline 2	15	-	-	-	-	-
Case 3	sawtooth	30	3	0.2	2.86	-	-
Case 4	sawtooth	30	9	0.6	8.53	-	-
Case 5	sawtooth	30	22.5	1.5	45	-	-
Case 6	slotted-sawtooth	30	9	0.6	8.53	0.5	15
Case 7	slotted-sawtooth	30	9	0.6	8.53	0.5	5

C. Simulation Setup

Preliminary Reynolds-averaged Navier-Stokes (RANS) numerical simulations have been carried out to further investigate and visualise the flow behaviour around serrated trailing edge of the tested airfoil. Airfoil simulations have been carried out for NACA 65(12)-10 at angles of attack 0°, 5° and 10° for a chord based Reynolds number of $Re_c = 3\times10^5$. The computational domain in the spanwise direction is 27 mm representing 20% of chord length and is equal to three wavelength of the serration enabling the use of periodic boundary conditions in the spanwise direction. The mesh approximately had 2.3 million elements and was created using snappyHexMesh supplied with OpenFOAM. The simulations were carried using OpenFOAM opensource code and SpalartAllmaras turbulence model. The airfoil wall was set to have a y^+ value of 30 used along with wall functions. The close to wall region of the airfoil was densely populated for the first 10 mm in-order to better capture the boundary layer.

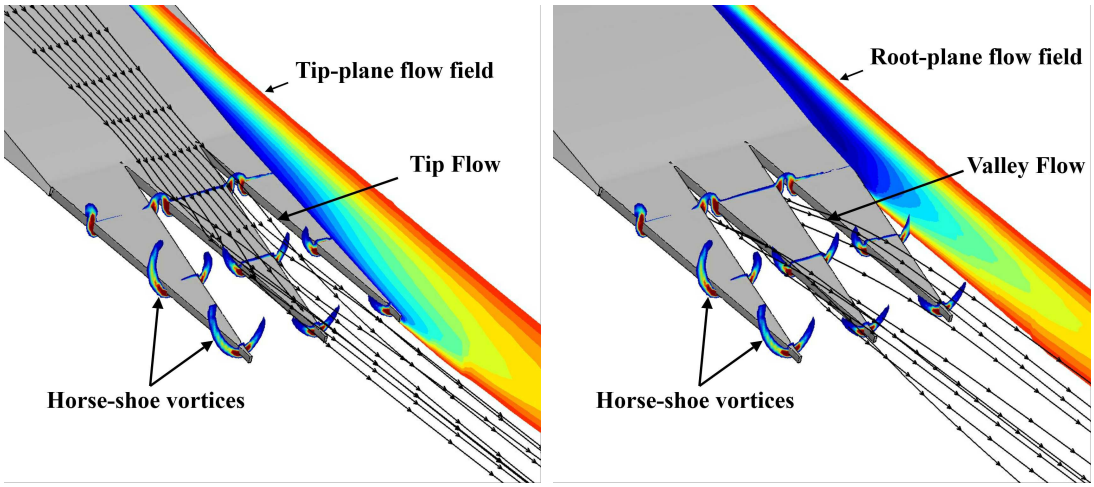

a) Tip Flow b) Root Flow

Fig. 3. Preliminary RANS results depicting the flow field over the serrations for $\alpha = 10°$ for chord based Reynolds number of $Re_c = 3\times10^5$.

III. Results

A. Aerodynamic Force Measurements

The lift and drag measurements of NACA 0012 and NACA 65(12)-10 airfoils for the Baseline, Blunt and Serrated configurations were carried out for a wide range of angles of attack and chord-based Reynolds numbers $Re_c = 2\times10^5$ to 6×10^5, corresponding to flow velocities of $U = 20$ m/s to $U = 60$ m/s. However, for the purpose of brevity the results for $Re_c = 3\times10^5$ and 5×10^5, corresponding to flow velocities $U = 30$ m/s and $U = 50$ m/s will be presented here. The tests were carried out for angles of attack (α) ranging from 0° to 20° and −5° to 20° for NACA 0012 and NACA 65(12)-10, respectively. The tested sawtooth serrations (Fig. 2a) had varying wavelengths of $\lambda = 3$ mm, 9 mm and 22.5 mm and amplitude $2h = 30$ mm. The slotted-sawtooth serrations (Fig. 2b) had a wavelength and amplitude of $\lambda = 9$ mm and $2h = 30$ mm along with slot width of $d = 0.5$ mm and two depths of $H = 5$ mm and 15 mm.

1. NACA 65(12)-10

The measured lift and drag coefficients for the three configurations of NACA 65(12)-10 airfoil are presented in Fig. 4. The upper two plots in Fig. 4 shows the force coefficients for two flow conditions with $Re_c = 3\times10^5$ (Fig. 4a) and 5×10^5 (Fig. 4b) and for airfoil with sawtooth serrations. The bottom two plots in Fig. 4 shows the force coefficients for similar flow conditions for airfoil with slotted-sawtooth serrations. The force measurement results for NACA 65(12)-10 airfoil with sawtooth serrations for the presented flow conditions show a reduction in lift coefficient of up to 15% for angles of attack ranging from −5° to 10° compared to the Baseline airfoil. NACA 65(12)-10 airfoil with slotted-sawtooth serrations shows an even greater reduction in lift coefficient of up to 30% for the entire range of angles of attack with the maximum reduction observed at lower angles of attack. Airfoils with trailing-edge serrations show increased lift coefficient in the pre-stall region but does not particularly change the stall behaviour of the airfoil. The results also show a prominent loss in lift coefficient for Blunt airfoil compared to Baseline airfoil which can be attributed to the decrease in surface area. The lift coefficient of the serrated airfoils shows a significant increase in lift

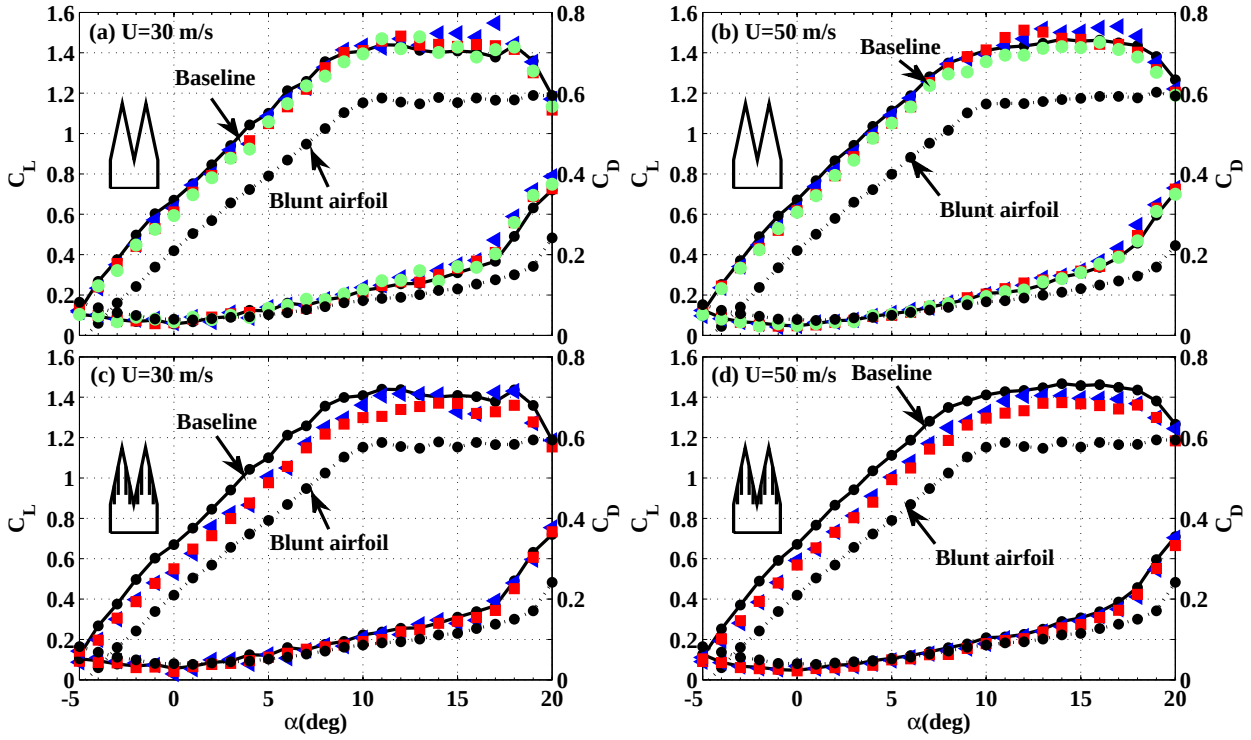

Fig. 4. Lift and drag coefficient results for NACA 65(12)-10 fitted with different serrations

(a) sawtooth serrations. Triangles: Red: λ = 22.5 mm; Blue: λ = 9 mm; Green: λ = 3 mm. (b) slotted-sawtooth serrations (λ = 9 mm, 2h = 30 mm ,d = 0.5 mm). Square: Blue: H = 5 mm; Red: H = 15 mm.

over the whole range of angles of attack in comparison with Blunt airfoil. The drag coefficient for the serrated airfoils are higher than that of the Baseline and Blunt airfoil, for angles of attack larger than 10°, it is also evident that the drag increases with increase in serration wavelength.

2. *NACA 0012*

The NACA 0012 airfoil force measurements for all the tested configurations are shown in Fig. 5. The lift coefficient results show noticeable difference in the overall behaviour of symmetric NACA0012 airfoil to that of the asymmetric NACA 65(12)-10. NACA 0012 airfoil fitted with serrations shows almost no reduction in lift coefficient, especially for small angles of attack, ranging from 0° to 9° showing that the effect of serrations on lift coefficient is less significant on NACA 0012 compared to that of NACA 65(12)-10, particularly at lower speeds with $Re_c = 3 \times 10^5$. The serrations significantly affect the maximum lift coefficient over the critical angles of attack ranges from 9° to 15°, but it appears to show improvement in the lift performance at deep stall angles from 17° to 20° and also increase the stall angle from 13° to 14° for $Re_c = 5 \times 10^5$. The lift perfomances for NACA 0012 airfoil with serration is similar to or better than the Blunt airfoil especially at high angles of attack. As mentioned earlier, based on the previous analytical and experimental results in [1, 4, 5, 11–13], sharp sawtooth (small α_s) and slotted-sawtooth serrations provide large and robust noise reduction over a wide frequency range. The aerodynamic results presented here, however, have revealed that such effective trailing-edge treatment (in term of noise) are prone to significant aerodynamic losses.

B. Wake Developement

Detailed flow measurements at several downstream wake locations have been performed using both LDA and PIV measurement techniques for NACA 65(12)-10 airfoil in order to better understand the effects of serration on the aerodynamic performance of the airfoil. The wake measurements were carried out at angles of attack, α = 0°, 5°, 10° and 15° for chord based Reynolds number $Re_c = 3 \times 10^5$ corresponding to a flow velocity of U = 30 m/s. For LDA the wake measurement were logged at downstream locations (Fig. 6) 0.2c, 0.3c, 0.5c, 1.0c, 1.5c and 2.0c relative to the trailing edge of the Baseline airfoil. Each measurement line was populated with 60 measurement points to accurately

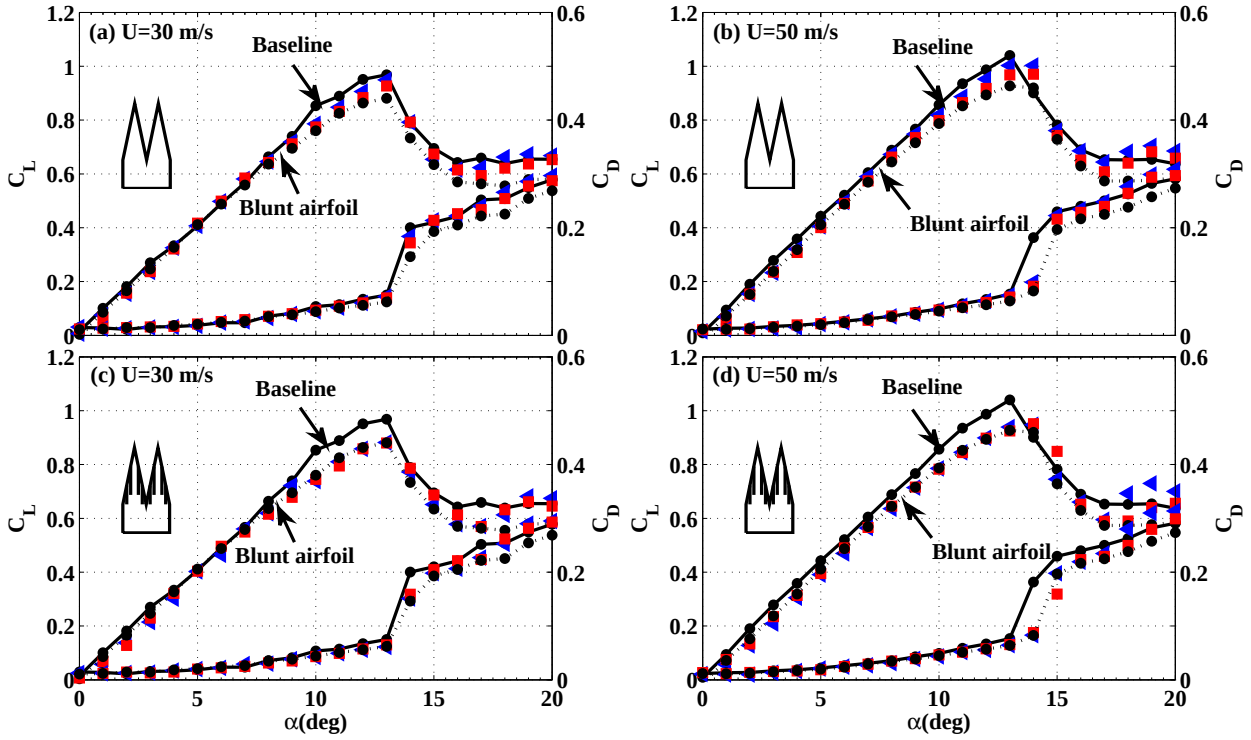

Fig. 5. Lift and drag coefficients for a NACA 0012 airfoil fitted with different serrations

Triangles: $\lambda = 9$ mm; squares: sawtooth serration with $\lambda = 3$ mm wavelength; pluses: slotted-sawtooth serration with $\lambda = 9$ mm, $d = 0.5$ mm and $H = 5$ mm; stars: slotted-sawtooth serration with $\lambda = 9$ mm, $d = 0.5$ mm and $H = 15$ mm.

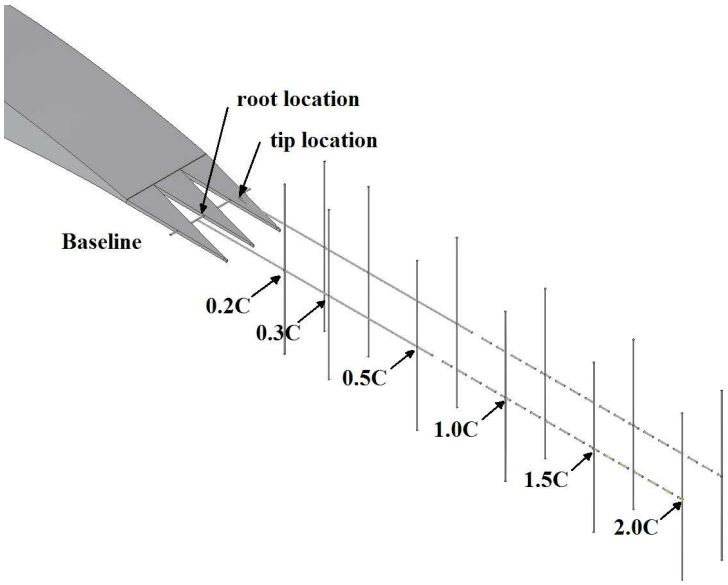

Fig. 6. Chord-wise locations used along the tip and root of the serration for LDA measurements.

capture the flow behaviour at the wake region. Results presented from Figs. 7 to 18 compare the flow behaviour between Baseline, tip and root locations of sawtooth serration ($\lambda = 9$ mm) and slotted-sawtooth serration ($\lambda = 9$ mm, $2h = 30$ mm, $d = 0.5$ mm and $H = 15$ mm) at different angles of attack.

The wake velocity profiles for baseline and serrated NACA 65(12)-10 airfoils at $\alpha = 0°$ are presented in Fig. 7. In the near-wake region, $x = 0.2c, 0.3c$ and $0.5c$, it can be observed that the flow at the tip position of the sawtooth

follows similar wake profile to that of the Baseline but with a slightly higher velocity deficit. The higher velocity deficit of the tip flow is due to the larger effective chord length of the tip flow. The dip location of the tip wake is the same as that of the Baseline flow. Unlike the tip flow, the flow from the root exhibits a very different behaviour. The root flow has a smaller velocity deficit, with the dip location moved upward due the flow through the serration valleys. The wake velocity deficit and the dip location at far-wake locations, $x = 1.0c, 1.5c$ and $2.0c$, gradually disappear between sawtooth and Baseline but it is evident from the results that the root flow can significantly change the nature of the wake development, even at small angles of attack. In the case of a NACA 65(12)-10 airfoil fitted with a slotted-sawtooth, the tip velocity deficit is notably larger than that of the Baseline and the standard sawtooth serration. The flow at the root position has also moved slightly upward compared to the sawtooth and Baseline. Results also show that the use of serrations in the case of a NACA 65(12)-10 at small angles of attack, lead to smaller flow deflection angle.

As shown in Figure 7 the flow behaviour in the case of an airfoil with straight TE is predominantly two dimensional, often with a strong ω_z vortex appearing near the TE due to flow separation on the airfoil upper surface. However, in the case of serrated airfoils, the presence of inclined lines (serrations) lead to significant change of the flow, introduction of three dimensional vortices due to the pressure difference over the serration, resulting in the appearance of effectively x-y layers of flow, which retain their properties for a large axial distance from the airfoil of particular interest here is to investigate.

The turbulent kinetic energy (TKE) profiles for NACA 65(12)-10 airfoil with treated and untreated trailing edges for $\alpha = 0°$ are presented in Fig. 8. In the vicinity of the trailing edge, $x = 0.2c, 0.3c$ and $0.5c$, it can be observed that the TKE magnitude of the sawtooth is similar to that of the Baseline. In the near-wake region, the TKE of the baseline airfoil shows a weak double peak behaviour due to the upper and lower boundary layers of the airfoil. The double-peak behaviour is even more evident for the tip-flow, due to the increase in the effective chord-length of the airfoil. The TKE of the root flow, however, peaks only in an area in the upper side of the airfoil, indicating the presence of an upward flow through the serration valleys. In the case of slotted-sawtooth, the peak due to the airfoil pressure-side boundary layer is much larger than that of the sawtooth serration. Results have also shown that in the far-wake region, $x = 1.0c, 1.5c$ and $2.0c$, the TKE for the airfoil fitted with sawtooth and slotted-sawtooth serrations is slightly wider, but generally match with the Baseline airfoil.

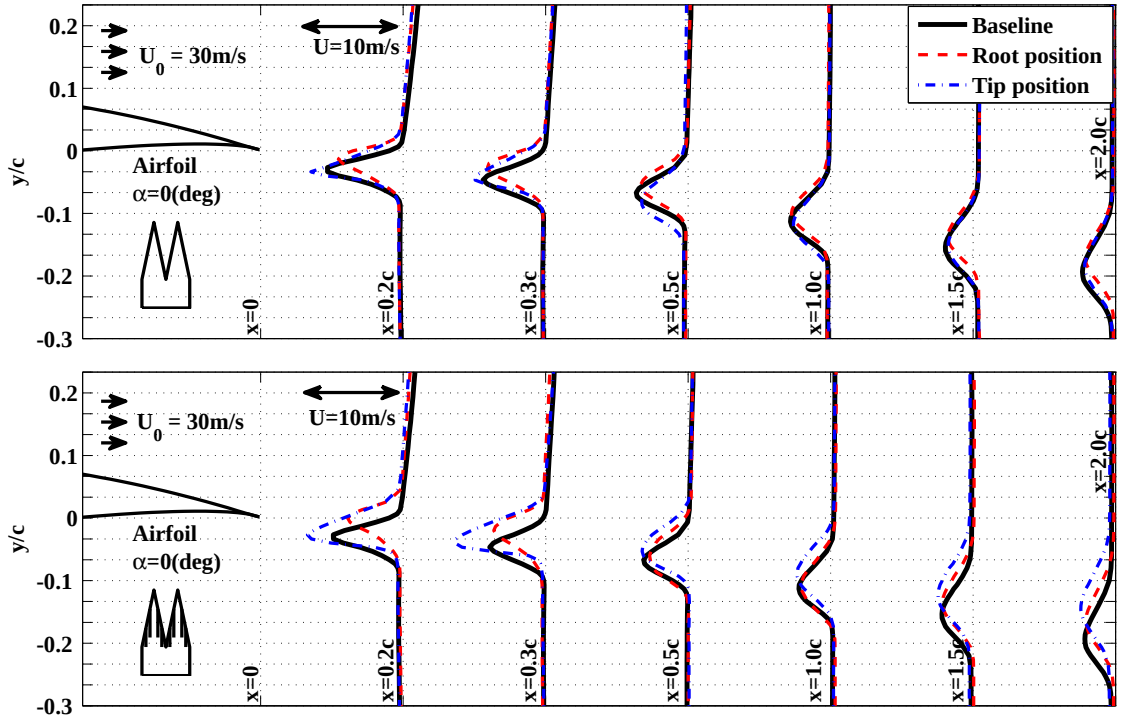

Fig. 7. Wake mean velocity for NACA 65(12)-10 airfoil at $\alpha = 0°$.

The Reynolds stress tensors profiles for NACA 65(12)-10 airfoil at $\alpha = 0°$ is presented in Fig. 9. The results show that the slotted-sawtooth has larger shear stress compared to the sawtooth at near wake locations, $x = 0.2c$ and $0.3c$.

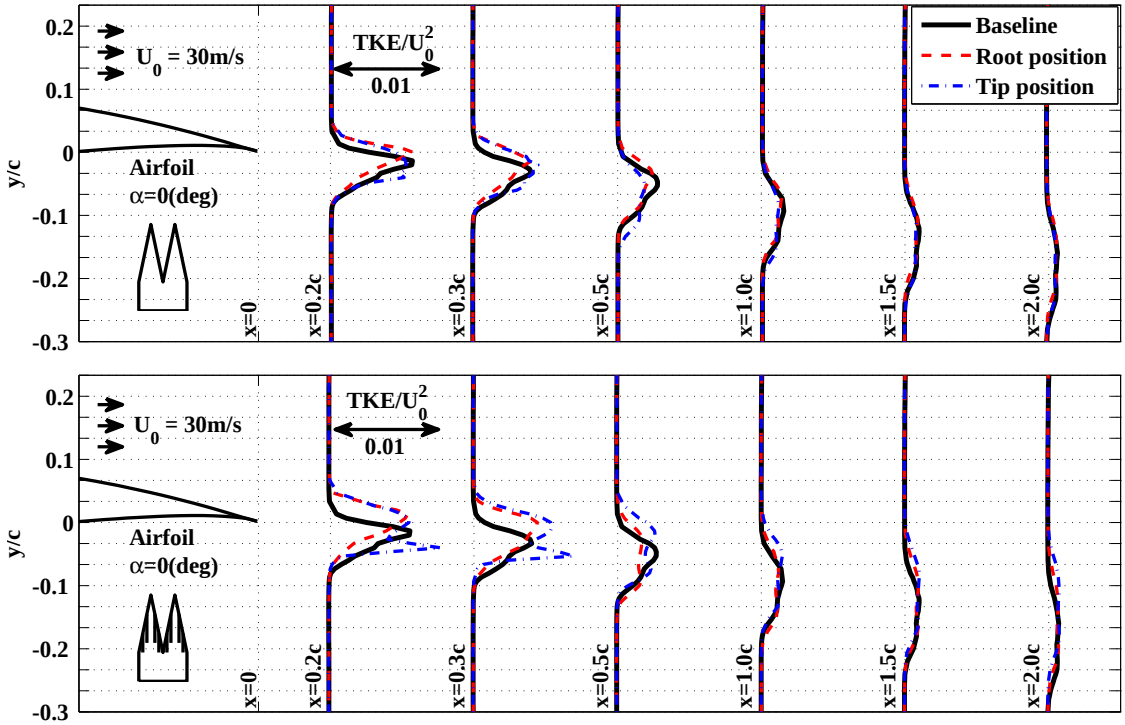

Fig. 8. Wake turbulent kinetic energy for NACA 65(12)-10 airfoil at $\alpha = 0°$.

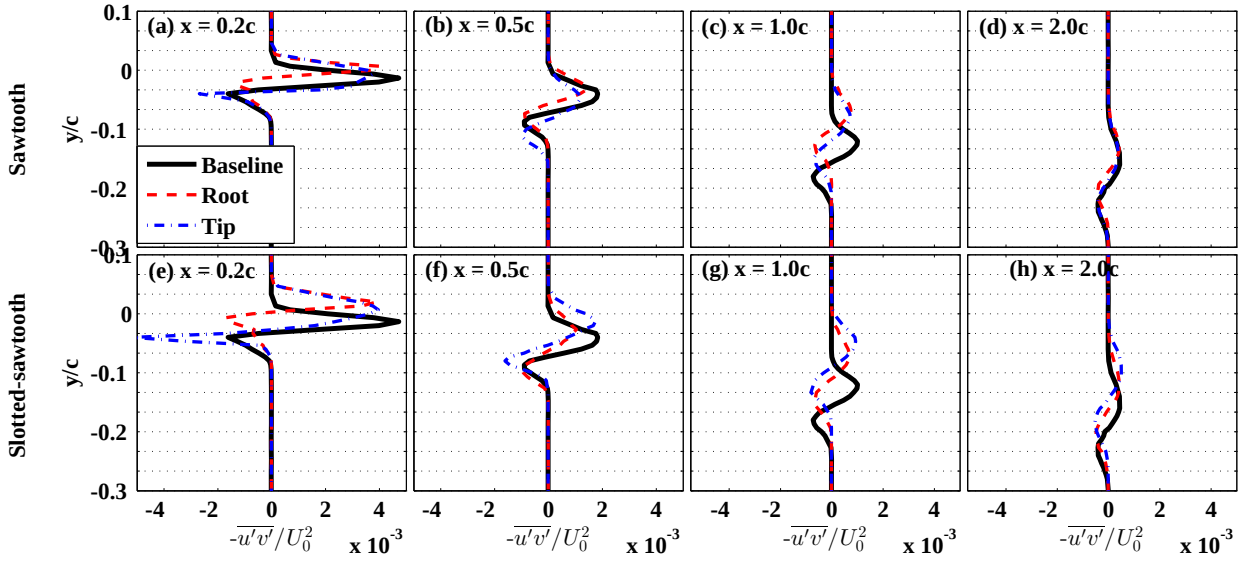

Fig. 9. Reynolds stress tensor for NACA 65(12)-10 airfoil at $\alpha = 0°$.

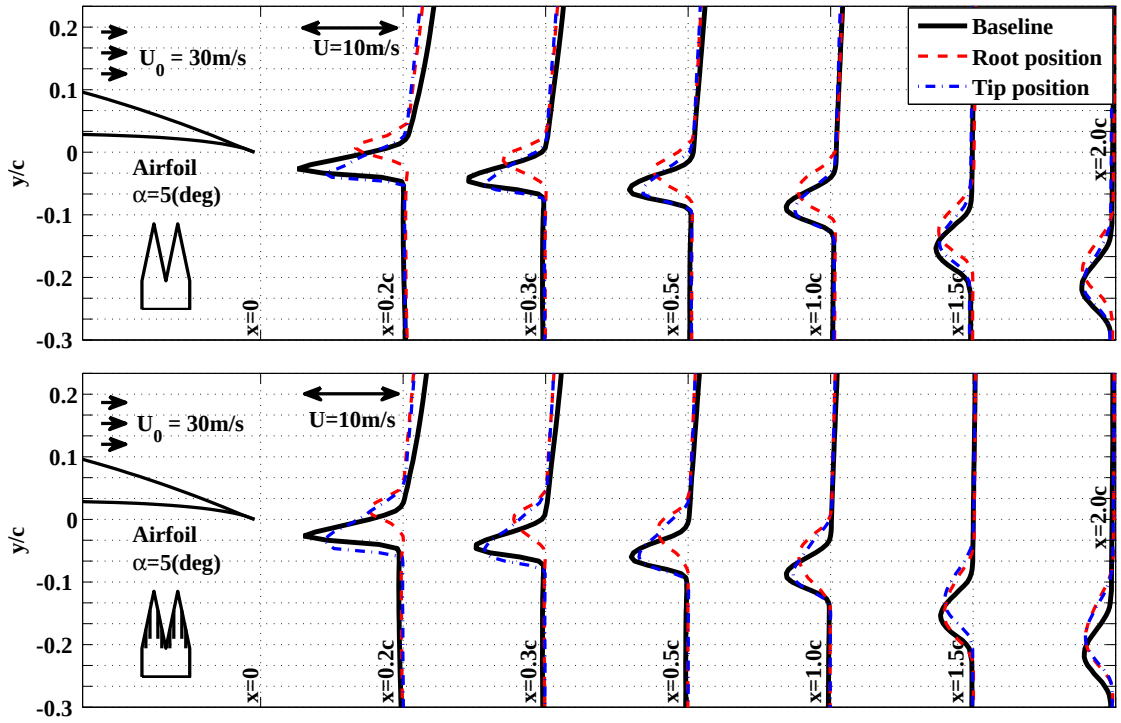

Fig. 10. Wake mean velocity for NACA 65(12)-10 airfoil at $\alpha = 5°$.

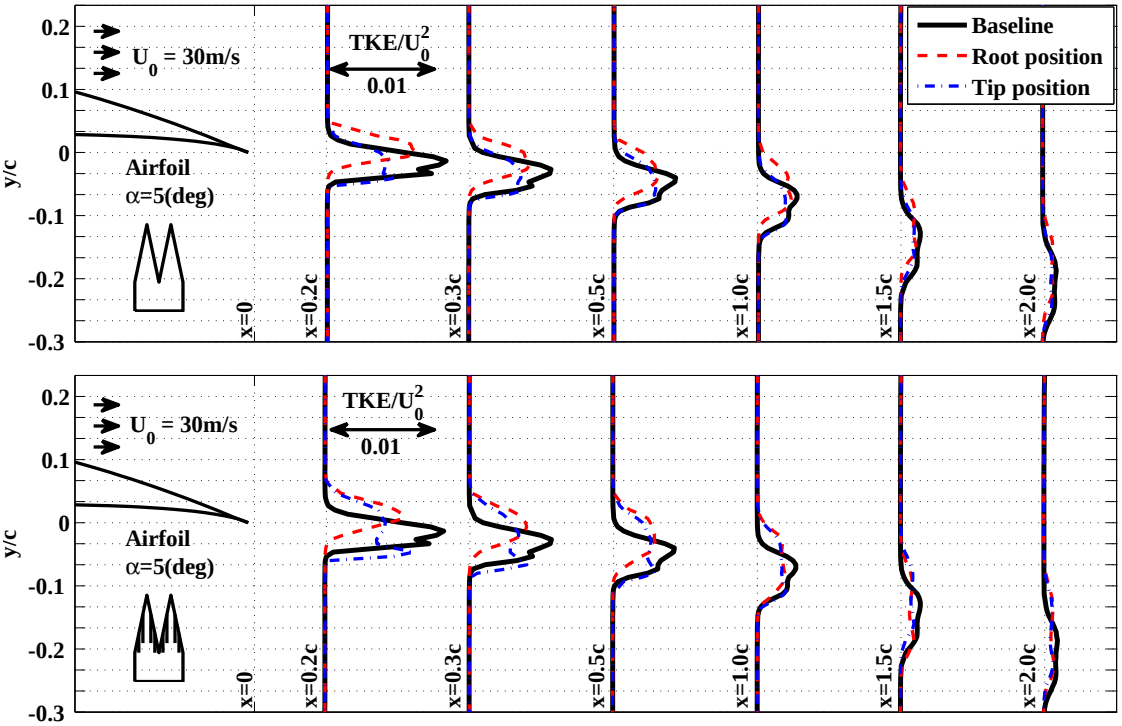

Fig. 11. Wake turbulent kinetic energy for NACA 65(12)-10 airfoil at $\alpha = 5°$.

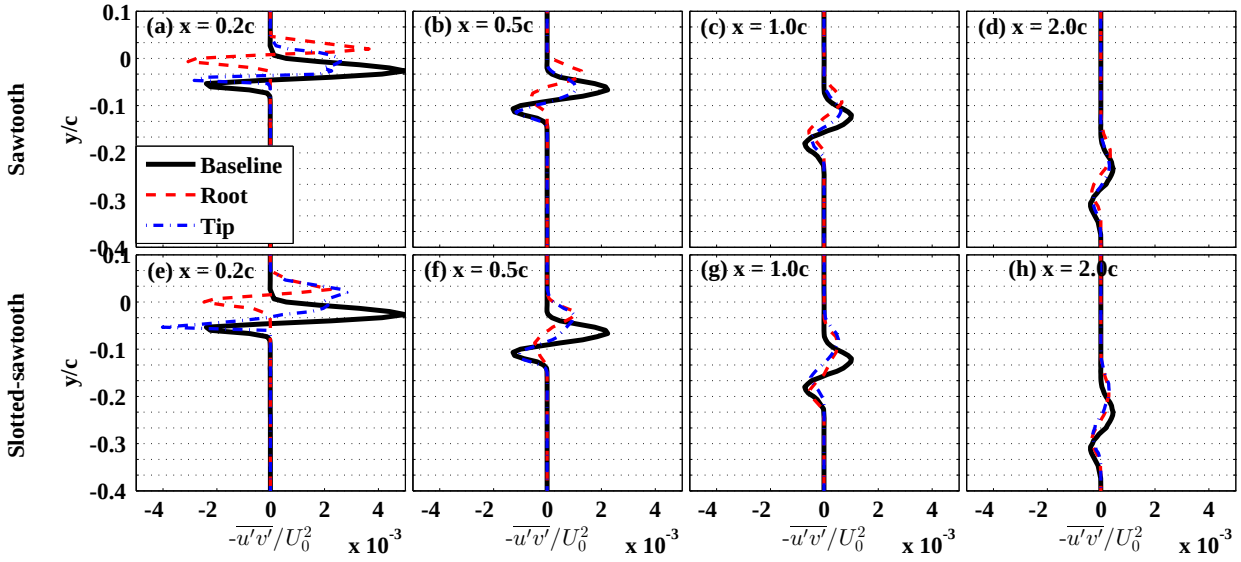

Fig. 12. Reynolds stress tensor for NACA 65(12)-10 airfoil at $\alpha = 5°$.

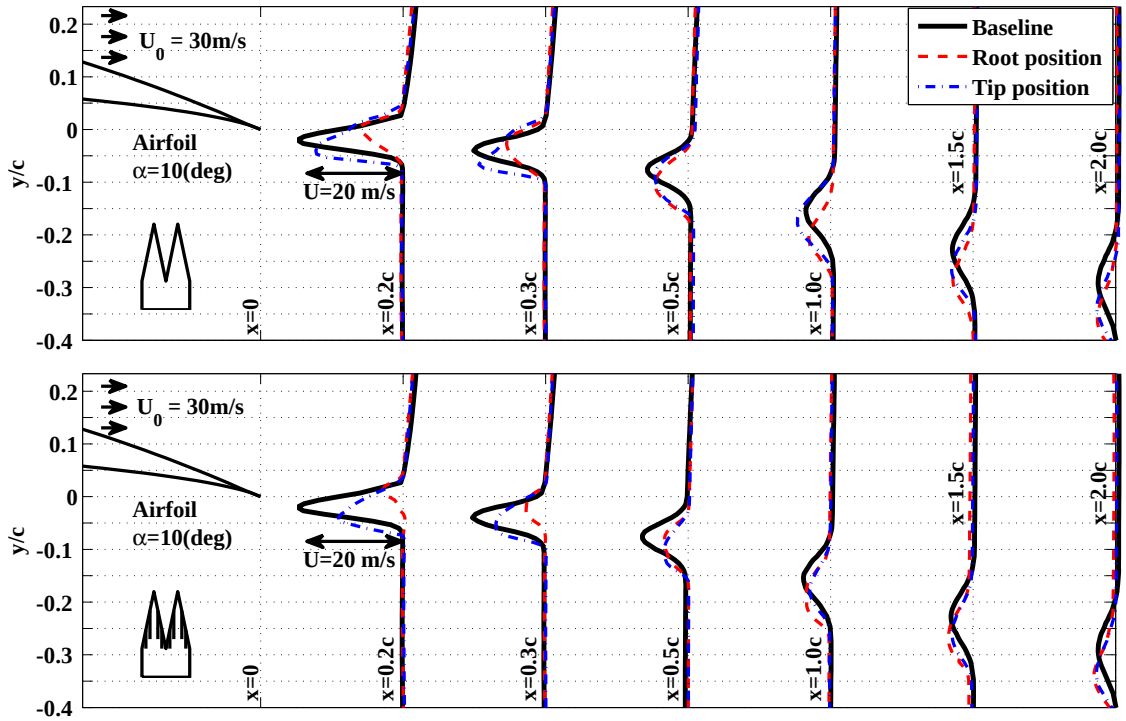

Fig. 13. Wake mean velocity for NACA 65(12)-10 airfoil at $\alpha = 10°$.

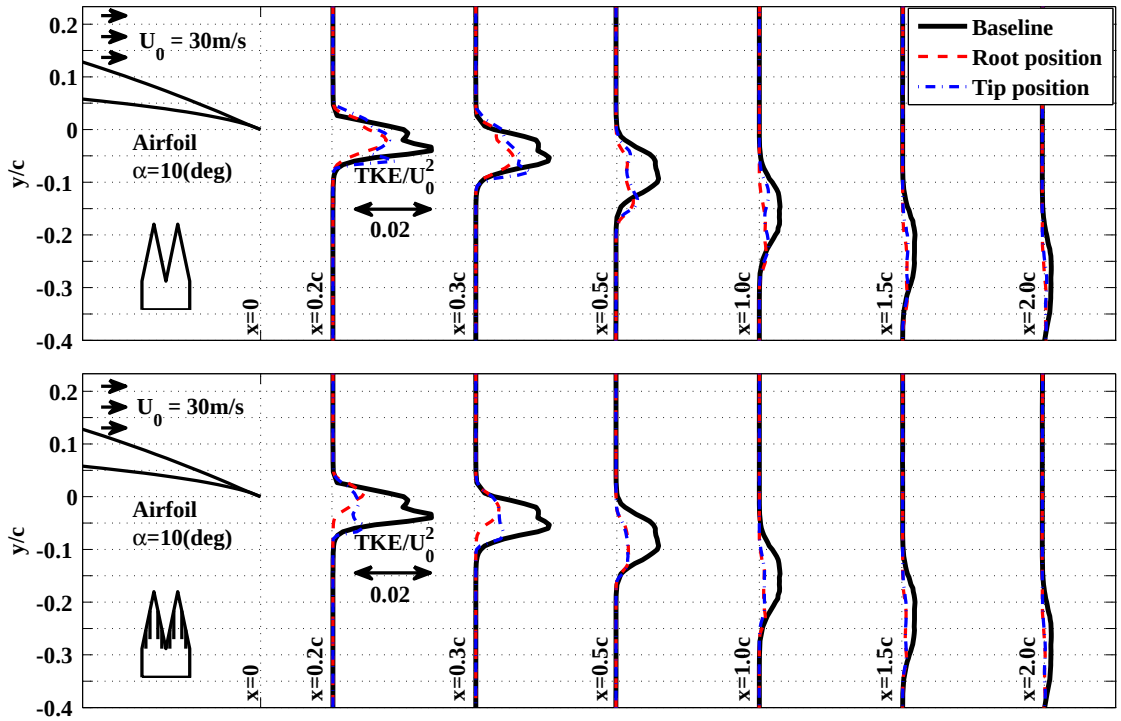

Fig. 14. Wake turbulent kinetic energy for NACA 65(12)-10 airfoil at $\alpha = 10°$.

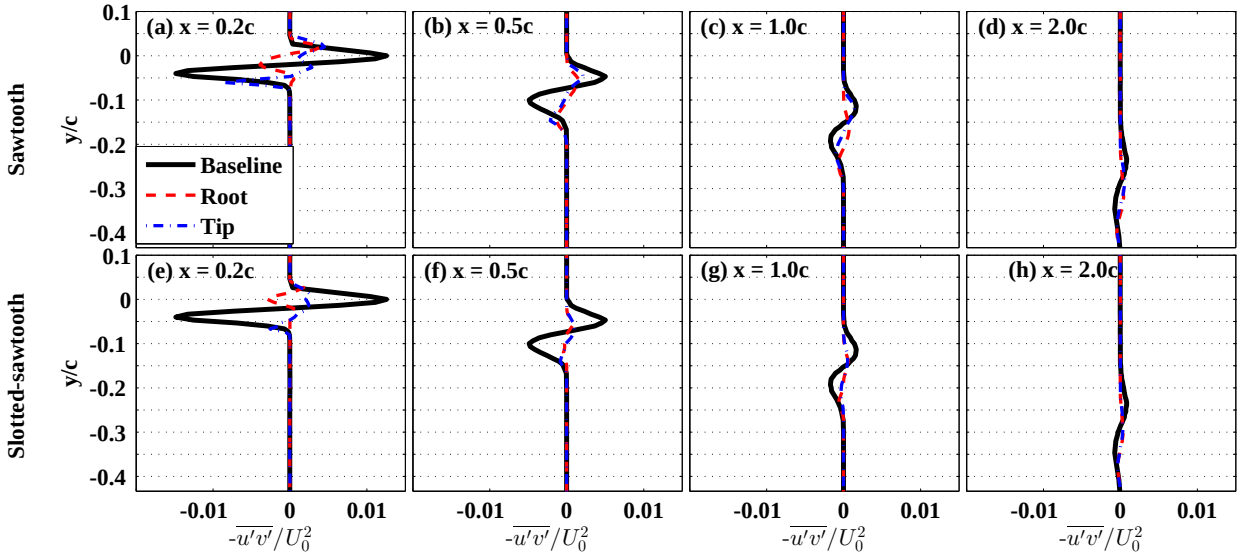

Fig. 15. Reynolds stress tensor for NACA 65(12)-10 airfoil at $\alpha = 10°$.

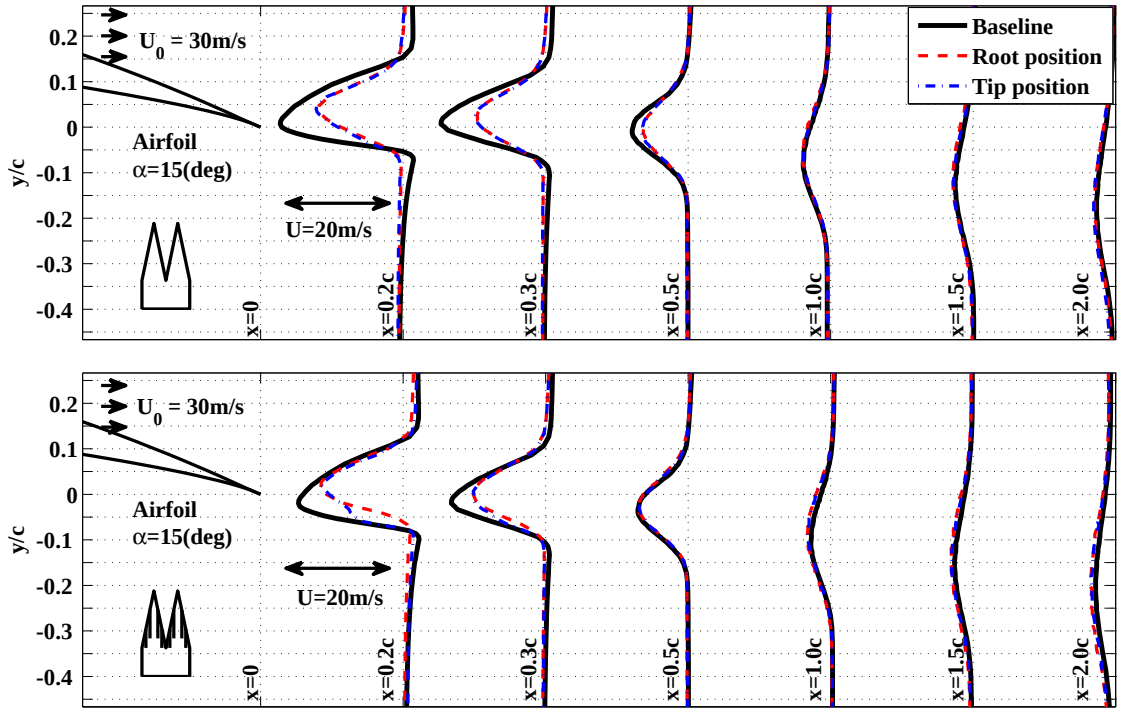

Fig. 16. Wake mean velocity for NACA 65(12)-10 airfoil at $\alpha = 15°$.

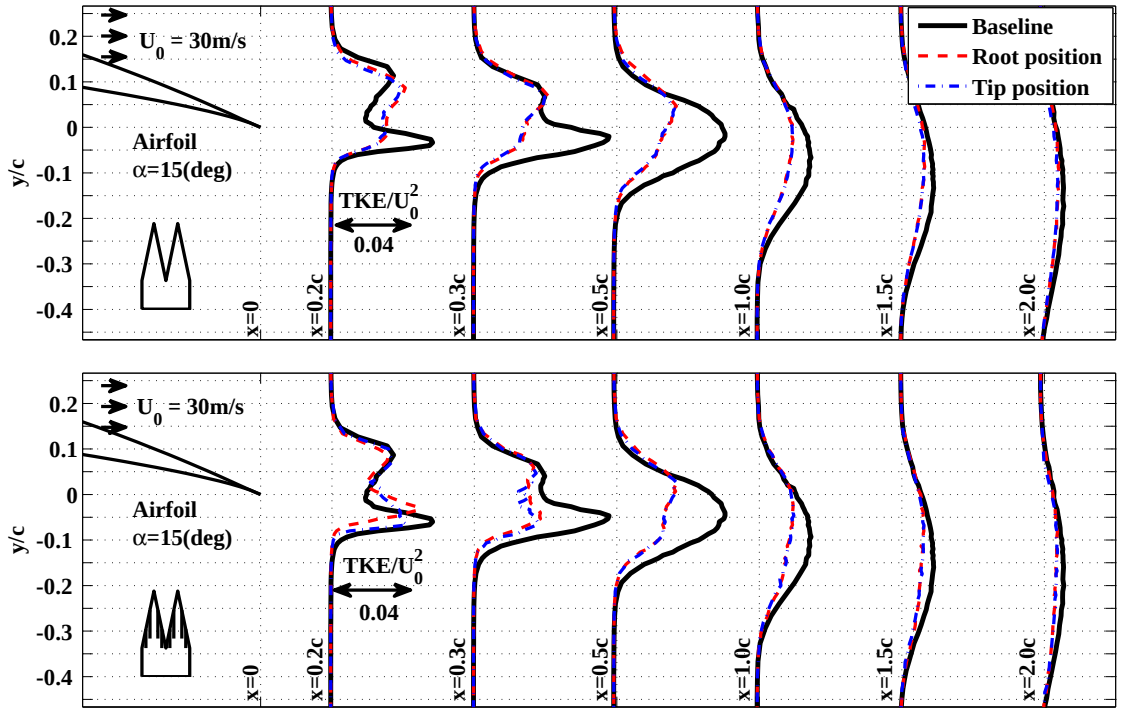

Fig. 17. Wake turbulent kinetic energy for NACA 65(12)-10 airfoil at $\alpha = 15°$.

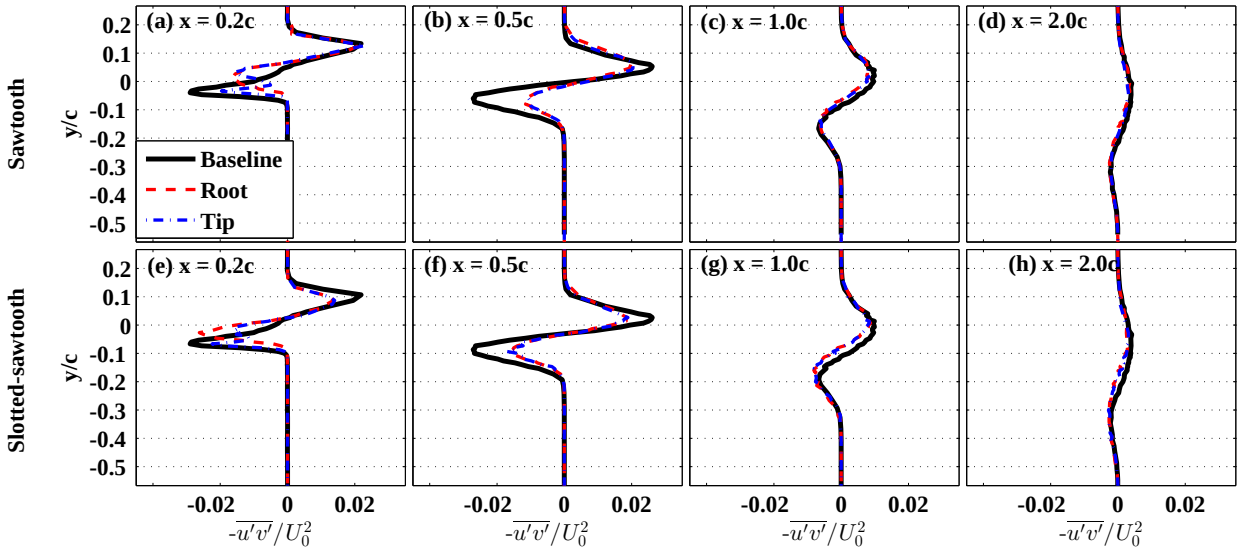

Fig. 18. Reynolds stress tensor for NACA 65(12)-10 airfoil at $\alpha = 15°$.

Figure 10 presents the results for the wake velocity profiles for the baseline and serrated NACA 65(12)-10 airfoils at $\alpha = 5°$. The wake velocity results here have shown that in the near-wake locations, $x = 0.2c, 0.3c$ and $0.5c$, unlike the results in Fig. 7 for $\alpha = 0°$, both the tip- and root-flows have much smaller velocity deficit, i.e. weaker wake, compare to the baseline case. In the case of the slotted-sawtooh, the root-flow has an even smaller velocity deficit than the normal sawtooth. As for $\alpha = 0°$, the root-flow dips in a region above the airfoils chord-line, signifying the presence of a relatively strong upward flow within the serration valleys. As seen in Figs. 7 and 10, the interaction of the strong upward root-flow and the tip-flow leads to an overall upward defection of the flow in the far-wake region compared to the baseline airfoil. This effect is more evident in the case of slotted-sawtooth airfoil.

The turbulent kinetic energy (TKE) profiles for NACA 65(12)-10 airfoil at $\alpha = 5°$ are presented in Fig. 11. The wake profiles of the baseline airfoil show a clear double-dip behaviour, which is due to the boundary layers on the pressure and suction sides of the airfoil. The near-wake results show that the use of serrations can lead to significant changes of the TKE of the flow. As observed before in Fig. 11, the root-flow has caused a region of high TKE above the chord-line. As a result, the high TKE region has enlarged along the y-axis. Results have also shown that the interaction of the root- and tip-flow results in a less turbulent far-wake.

The wake velocity profiles, TKE results and the Reynolds shear stress for the NACA 65(12)-10 airfoil at $\alpha = 10°$ with and without serrations are presented in Figs. 16 to 18, respectively. The near wake results ($x = 0.2c, 0.3c$ and $0.5c$) show that at high angles of attack, the difference between the tip and root flows increases and unlike the results at small AoAs, after mixing the resultant flow has shifted downwards compared to the baseline flow. It can also be seen that in the near wake, the flow from slotted-sawtooth has less velocity deficit than the sawtooth serration, leading to significant reduction of the TKE with the $x/c = 0$ to 0.5. One can, therefore, conclude from the velocity results that the use of serration at high AoAs (before stall), can significantly change the wake structure by reducing the velocity deficit. This is believed to be mainly due to the root flow and the planar interaction occurring between the tip and root flow in the vicinity of the trailing edge. As seen in Figs. 14 and 15, the TKE and shear stress term drop significantly to a very small value within a short distance from the trailing edge. This is a very interesting find as the fan flow interaction with OGVs is an important part of the fan noise and fan blades and compressors are often operated at high angles of attack, before stall, when the turbulent boundary layer is on the point of becoming early separation. Similarly, in the case of contra-rotating propeller, minimizing the energy content of the flow from the front row blades can significantly reduce the noise from the interaction of the wake flow with the rear row blades.

Results in Fig. 16 present the wake flow velocity for a NACA 65(12)-10 airfoil at $\alpha = 15$. The results at $x/c = 0.2$ show the appearance of a large wake, indicating the presence of early separation on the suction side of the airfoil (reference to flow visualizations later). Unlike the results at smaller AoAs, the root and tip velocity profiles are very similar, but showing much smaller deficit compared to the baseline case in the near wake region. The velocity profiles, however, converge to that of the baseline after $x/c = 1.0$. The TKE results in Fig. 17 also show that the use of serration can lead to significant reduction of the energy content of the wake along and near the chord-line, but has very little effect further up inside the wake caused by the airfoil early separation. It is discussed later that this is due to the

emergence of a new vorticity, formed as a result of the interaction of the flow on the airfoil pressure-side with an highly angled serrated surface. Results also show that for the case of high AoA, very little difference can be observed between the normal and slotted sawtooth serrations. The results presented in Fig. 18 also show that the sawtooths do not particularly change the Reynolds shear stress in the near wake and results converge to that of the baseline after $x/c = 1.0$.

In order to improve our understanding of the flow behaviour around the serrations and the wake development, in this section some PIV results obtained in the airfoil near wake regions $x/c = 0$ to 0.6 and are presented in Figs. 19 and 20. As seen earlier in Figs. 7 to 18, the flow around the airfoil at small angles of attack remains almost streamline near the trailing-edge to a large extend, forming only a small wake width. As mentioned previously, at small angles of attack, using serrations does not particularly reduce the TKE in the wake, but may move the peak position, i.e. velocity dip, upward due to the flow moving upward from the serration valleys. However, at higher AoAs, where maximum lift can be obtained and noise reduction is of interest, the wake becomes much larger and the effect of the serrations also becomes more evident. At high AoA, the interaction of the flow over the pressure side of the airfoil and the serrations leads to the formation of new complex vorticity that are studied here. PIV results are provided for the baseline, blunt and serrated NACA 0012 airfoil at $U = 30$ m/s.

At moderately high AoA, $\alpha = 10°$, the flow over the pressure and suction sides of the baseline airfoil remain nearly streamline, resulting in a small boundary layer at the TE and a narrow wake. In the case of serrated airfoil, while the flow along the tip-line of the serration remain streamline, the root flow moves upward within the valley, causing a three-dimensional flow before $x/c = 0.2$. As seen earlier in Fig. 14, the emergence of this three-dimensional near-wake flow, has resulted in high dissipation of the TKE, such that the TKE at $x/c = 1.0$ reaches almost that of the free-stream flow. As seen earlier in Fig. 5, the emergence of the new vortex, working against the separation vortex can also improve the aerodynamic performance of the airfoil by producing some lift, making the separation vortex smaller and changing its structure.

As seen in Fig. 20, in the case of early separation at high angles of attack ($\alpha = 15°$), there exists a large vortex above the trailing edge. The flow field over the baseline and blunt airfoils are principally the same. However, the use of serration appears to have completely changed the flow field in the regions $x/c = 0$ to 0.2. The flow from the airfoil lower surface passing through the serration valleys causes a secondary vorticity (valley vorticity), spinning in the opposite direction of the separation vorticity. Results show that the strong flow originating from the serration root, has made the main vorticity much smaller and has moved the center of the vorticity from $x/c = 0.2$ to around $x/c = 0$. As observed in Fig. 17, the interaction of the two contra-rotating vortices causes significant reduction of the TKE along chord-line in the wake, particularly within regions $x/c = 0$ to 1.0. This can be attributed to the shift of the vortex-eye further upstream and higher level of dissipation as a results of two contra-rotating vortices interacting with each other. As seen in Figs. 20 and 21, the shape and location of the root vortex changes along the span over the serrations. The valley vortex is particularly large in the middle of serration valley, with its centre near the root, and it gets smaller and moves downstream at the tip location. Results have also shown that the location of the valley vortex depends strongly on the serration geometry. Figure 21 shows slice view of velocity contours over the serrations, the results show the development of spanwise vortices and the horse-shoe structures much more clearly. Results obtained using sharp serrations ($\alpha_s = 8.53°$) shows that the vortex valley will mainly over the valley region and within $x/c = 0$ to 0.2, while in the case of wide serrations ($\alpha_s = 45°$) the valley vortex occurs at $x/c = 0.2$, makes much less effective for moving the separation vortex and reducing the TKE in the near wake. The comparison of the results here and those presented in Fig. 4, also show that the increase in the lift coefficient observed at $30m/s$ at high angles of attack, particularly for sharp serrations ($\lambda = 9mm$), can be attributed to the upward force caused by the emergence of the valley vortex and the changes consequently occurred to the separation vortex. Therefore, it can be concluded that the size and location of the valley vortex can determine the level of lift increase compared to the baseline airfoil.

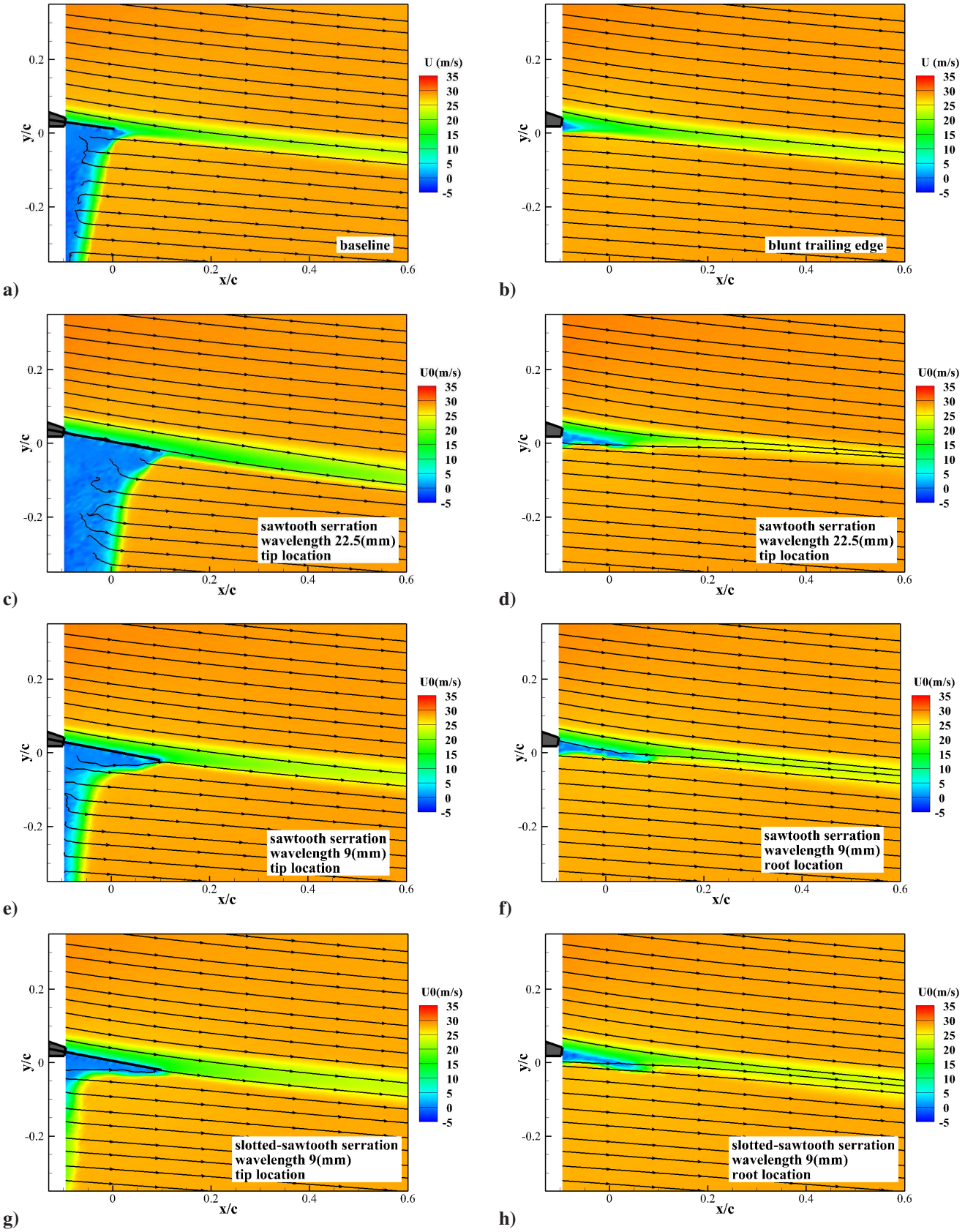

Fig. 19. Veolicty contours from PIV for NACA 0012 airfoil at $\alpha = 10°$.

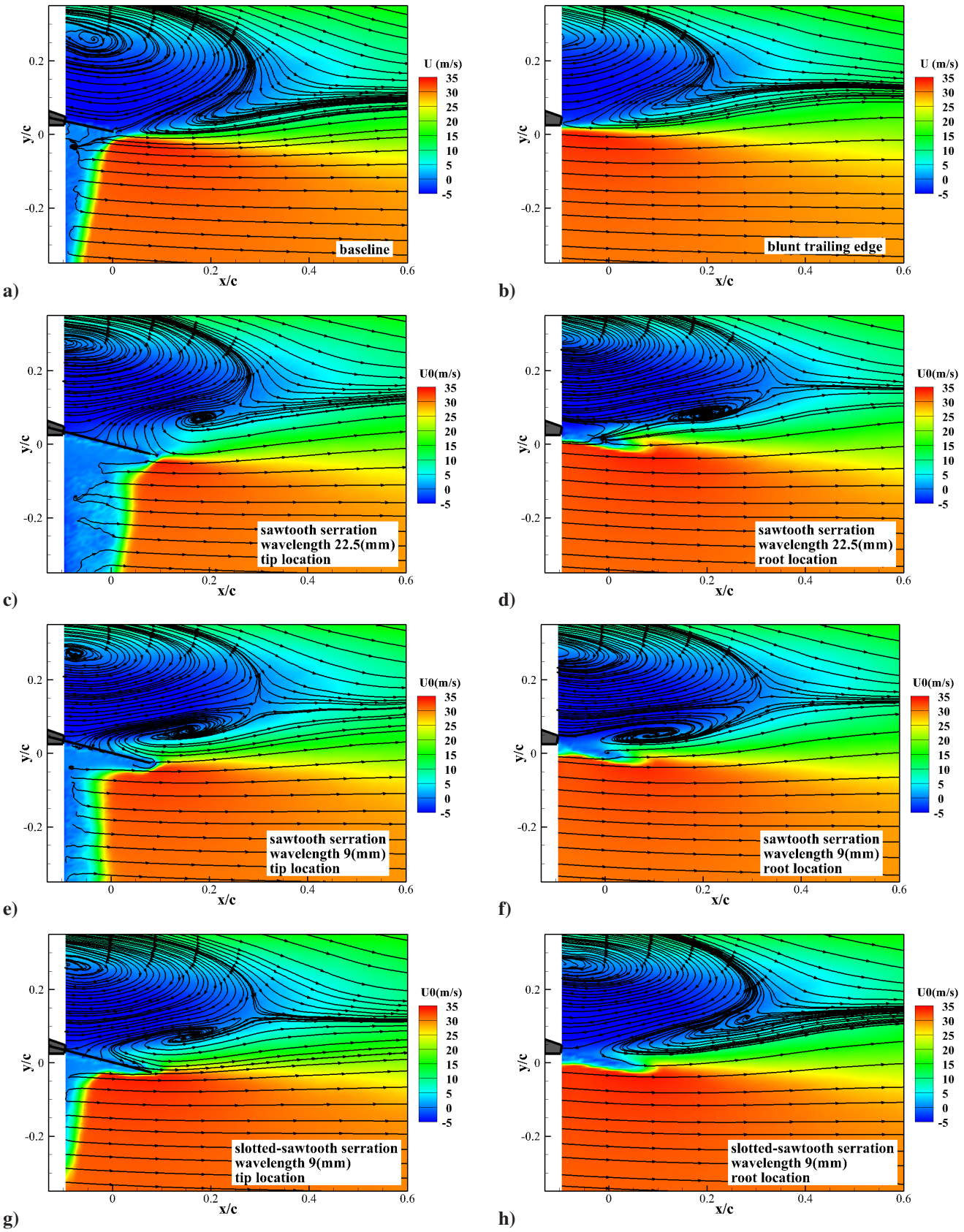

Fig. 20. Veolicty contours from PIV for NACA 0012 airfoil at $\alpha = 15°$.

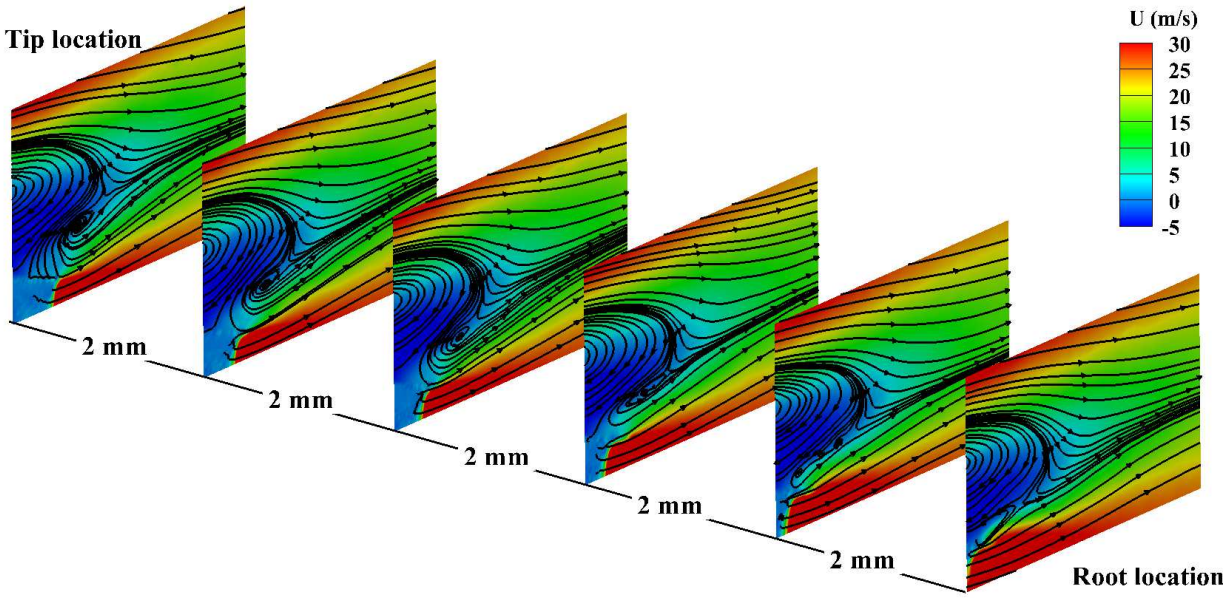

Fig. 21. Slice view of velocity countours over the sawtooth serration for NACA 0012 at angle of attack $\alpha = 15°$

C. Wake Energy Content

The flow behaviour over the trailing edge and wake was studied in the preceding sections. In addition to the general velocity and turbulent kinetic energy information obtained using the PIV and LDV results, frequency energy content of the wake turbulence can also provide us with some valuable information, especially in the context of wake-interaction noise. The velocity and velocity power spectral density (PSD) results have been obtained using a single hotwire probe, traversed within the wake, see Sec. II. Velocity PSD results are provided for the NACA 65(12)-10 airfoil at different angles of attack ($\alpha = 0°$, $5°$, $10°$ and $15°$), at flow speed of $U = 20m/s$, at two axial locations, $x/c = 0.2$ and 0.5. The PSD results, at each location and frequency, are normalized by the PSD results of the baseline airfoil.

The relative PSD results at small angles of attack ($\alpha = 0°$ and $5°$) show the emergence of two distinct high energy regions above the chord-line, one centred around 50Hz and the second one around 4000Hz. As observed in Figs. 7 and 8, this is believed to be mainly due the upward shift of the flow at small angles of attack, caused by the serration valley flow. The upward flow also causes significant velocity PSD reduction in the areas along and below the chord-line over the entire frequency range. Similar trends have also been observed in the case of $\alpha = 10°$. The comparison of the standard serration and slotted-sawtooth shows very little difference. At high angles of attack, $\alpha = 15°$, the PSD trends change completely. Results have shown an area of reduced velocity PSD above the chord-line and two distinct areas of PSD increase below the chord-line. As discussed earlier for the velocity and TKE results at high angles of attack, Figs. 16 and 17, the valley flow completely changes the wake behaviour below the chord-line, which is also consistent with the results in Fig. 22. The results in Fig. 22 are particularly important as the velocity energy spectrum is one of the main parameters used as input for leading edge noise models, such as Amiets model. From the results in Fig. 22 it can be concluded that the use of serrations at small or moderate pre-stall angles of attack, leads to an increase of energy above the chord-line and decrease below the chord-line, while that reverses at post-stall angles.

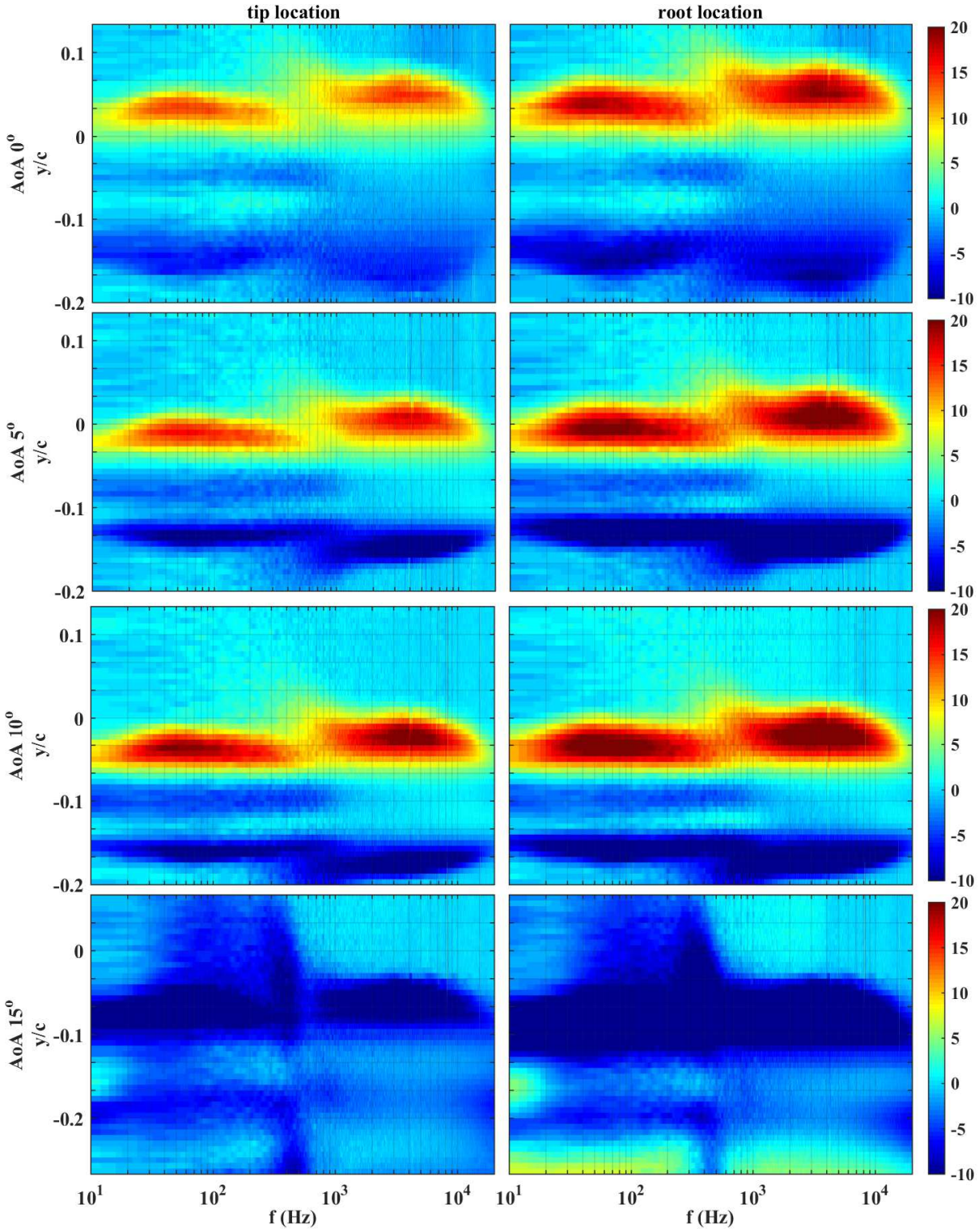

Fig. 22. Normalised velocity PSD for NACA 65(12)-10 airfoil at location $x = 0.2c$.

IV. Conclusions

Experimental study on NACA 0012 and NACA 65(12)-10 attached with serrated trailing edges have been carried out to better understand their aerodynamic and aeroacoustic performance. The experimental results show that the trailing edge serration can change the aerodynamic performances significantly. The level of performance change depends on the type of airfoil and the geometrical characteristics of the serration. Eventhough the $C_L - \alpha$ curve trend is not affected by the serrations the lift coefficient is affected and the post stall characteristics of the airfoil is changed. The flow field results show that the serrations significantly affect the velocity dip location and velocity deficit compared to the Baseline. The velocity profiles vary notably between the tip and root profiles that would cause significant shear stress between the tip and root planes. The velocity dip location shows an upward shift in the wake profiles at the root positions relative to the baseline and the tip positions. This indicates that the flow originating from the pressure surface passes through the airfoil root through the serration valleys moving upwards like a jet flow. The wake turning (downwash) angle for the root positions are significantly lesser than that of the Baseline and tip positions. This shows the flow field over the serration is predominantly three dimensional with strong vortices present in the spanwise and streamwise direction. This three dimensional flow and vortices influences the turbulent energy decay at the wake region bring down the turbulence level significantly compared to the baseline at about $x = 0.5c$. This is very important when considering noise generated from fan flow interaction with OGV since the inlet turbulence plays a major role in airfoil self noise. Moreover since the fan blades are operated at high angles of attack the reduction in inlet turbulence will aid delay the flow separation. Wake energy content results showed that at small or moderate pre-stall angles of attack leads to an increase of energy above the chord-line and decrease below the chord-line, while that reverses at post-stall angles.

Acknowledgments

The technical support and advice provided by Dr. Raf Theunissen for experimental setup is gratefully acknowledged. M.A. would like to acknowledged the financial support provided by the Royal Academy of Engineering.

References

[1] Hardin, J. C., "Airframe self-nosie - four years researchitle," *NASA Tech Memo*, 1976.

[2] Brooks, T., Pope, D., and Marcolini, M., "Airfoil self-noise and prediction," *NASA Reference Publication 1218*, 1989, pp. 142.

[3] Williams, J. E. F. and Hall, L. H., "Aerodynamic sound generation by turbulent flow in the vicinity of a scattering half plane," *Journal of Fluid Mechanics*, Vol. 40, 1970, pp. 657.

[4] Howe, M. S., "Noise produced by a sawtooth trailing edge," *The Journal of the Acoustical Society of America*, Vol. 90, No. 1, 1991, pp. 482.

[5] Gruber, M., Azarpeyvand, M., and Joseph, P., "Airfoil trailing edge noise reduction by the introduction of sawtooth and slitted trailing edge geometries," *Proceedings of 20th International Congress on Acoustics*, 2010, pp. 1–9.

[6] Jones, L. and Sandberg, R., "Numerical Investigation of Airfoil Self-Noise Reduction by Addition of Trailing-Edge Serrations," *16th AIAA/CEAS Aeroacoustics Conference*, 2010, pp. 1–23.

[7] Fernandes, G. C., Weinmann, M., and Sandberg, R. D., "Applicability of RANS models for accurate computation of flow over airfoils with serrated trailing edges," *5th European Conference on Computational Fluid Dynamics, ECCOMAS CFD 2010*, 2010, pp. 14–17.

[8] Sandberg, R. D. and Jones, L. E., "Direct numerical simulations of low Reynolds number flow over airfoils with trailing-edge serrations," *Journal of Sound and Vibration*, Vol. 330, No. 16, 2011, pp. 3818–3831.

[9] Jones, L. E. and Sandberg, R. D., "Acoustic and hydrodynamic analysis of the flow around an aerofoil with trailing-edge serrations," *Journal of Fluid Mechanics*, Vol. 706, 2012, pp. 295–322.

[10] Moreau, D., Brooks, L., and Doolan, C., "On the noise reduction mechanism of a flat plate serrated trailing edge at low-to-moderate Reynolds number," *18th AIAA/CEAS Aeroacoustics Conference (33rd AIAA Aeroacoustics Conference)*, 2012, pp. 1–20.

[11] Gruber, M., *Aerofoil noise reduction by edge treatments*, Doctoral thesis, University of Southampton, 2012.

[12] Gruber, M., Joseph, P. F., and Azarpeyvand, M., "An experimental investigation of novel trailing edge geometries on airfoil trailing edge noise reduction," *19th AIAA/CEAS Aeroacoustics Conference*, Berlin, Germany, 2013, pp. 1–23.

[13] Azarpeyvand, M., Gruber, M., and Joseph, P. F., "An analytical investigation of trailing edge noise reduction using novel serrations," *19th AIAA/CEAS Aeroacoustics Conference*, Berlin, Germany, 2013, pp. 1–17.

[14] Chong, T. P. and Joseph, P. F., "An experimental study of airfoil instability tonal noise with trailing edge serrations," *Journal of Sound and Vibration*, Vol. 332, No. 24, 2013, pp. 6335–6358.

[15] Chong, T. P., Joseph, P. F., and Gruber, M., "Airfoil self noise reduction by non-flat plate type trailing edge serrations," *Applied Acoustics*, Vol. 74, No. 4, 2013, pp. 607–613.

[16] Liang, J., Weiyang, Q., Liangfeng, W., Fan, T., and Weijie, C., "Experimental and Numerical Study on Noise Reduction Mechanisms of an Airfoil with Serrated trailing edge," *20th AIAA/CEAS Aeroacoustics Conference*, Atlanta, GA, 2014, pp. 1–18.

[17] Sanjosé, M., Méon, C., Masson, V., and Moreau, S., "Direct numerical simulation of acoustic reduction using serrated trailing-edge on an isolated airfoil," *20th AIAA/CEAS Aeroacoustics Conference*, Atlanta, GA, 2014, pp. 1–15.

[18] Lau, A. S. H., Haeri, S., and Kim, J. W., "The effect of wavy leading edges on aerofoil-gust interaction noise," *Journal of Sound and Vibration*, Vol. 332, No. 24, 2013, pp. 6234–6253.

[19] Liu, X., Azarpeyvand, M., and Theunissen, R., "On the Aerodynamic Performance of Serrated Airfoils," *22nd International Congress on Sound and Vibration*, Florence, italy, 2015, pp. 12–16.

[20] Liu, X., Kamliya Jawahar, H., Azarpeyvand, M., and Theunissen, R., "Aerodynamic and Aeroacoustic Performance of Serrated Airfoils," *21st AIAA/CEAS Aeroacoustics Conference*, Dallas, TX, 2015, pp. 1–16.

[21] Chong, T. P. and Vathylakis, A., "On the aeroacoustic and flow structures developed on a flat plate with a serrated sawtooth trailing edge," *Journal of Sound and Vibration*, Vol. 354, 2015, pp. 1–26.

[22] Avallone, F., Arce Leon, C., Pröbsting, S., Lynch, K., and Ragni, D., "Tomographic-PIV investigation of the flow over serrated trailing-edges," *AIAA SciTech/ 54th AIAA Aerospace Sciences Meeting*, San Diego, California, 2016, pp. 1–14.

[23] Lyu, B., Azarpeyvand, M., and Sinayoko, S., "Prediction of noise from serrated trailing-edges," *Journal of Fluid Mechanics*, Vol. 793, 2016, pp. 556–588.

[24] Vathylakis, A., Chong, T. P., and Joseph, P. F., "Poro-Serrated Trailing-Edge Devices for Airfoil Self-Noise Reduction," *AIAA Journal*, Vol. 53, No. 11, 2015, pp. 1–16.

[25] Herr, M. and Dobrzynski, W., "Experimental Investigations in Low-Noise Trailing-Edge Design," *AIAA Journal*, Vol. 46, No. 6, 2005, pp. 1167–1175.

[26] Finez, A., Jondeau, E., Roger, M., and Jacob, M. C., "Broadband noise reduction with trailing edge brushes," *Proceedings of the 16th AIAA/CEAS aeroacoustics conference*, 2010, pp. 1–13.

[27] Oerlemans, S., Fisher, M., Maeder, T., and Kögler, K., "Reduction of wind turbine noise using optimized airfoils and trailing-edge serrations," *AIAA Journal*, Vol. 47, No. 6, 2009, pp. 1470–1481.

[28] Boutilier, M. S. H., *Experimental Investigation of Transition over a NACA 0018 Airfoil at a Low Reynolds Number*, Master of applied science, University of Waterloo, 2011.

[29] Theunissen, R., Di Sante, a., Riethmuller, M. L., and Van Den Braembussche, R. a., "Confidence estimation using dependent circular block bootstrapping: Application to the statistical analysis of PIV measurements," *Experiments in Fluids*, Vol. 44, No. 4, 2008, pp. 591–596.